SAND99-3090 J

November 14, 1996

PERMEABILITY OF WIPP SALT DURING DAMAGE EVOLUTION AND HEALING*

Kwai S. Chan and Sol R. Bodner+
Southwest Research Institute, San Antonio, TX 78238

Darrell E. Munson
Sandia National Laboratories**, Albuquerque, NM 87185

ABSTRACT

The presence of damage in the form of microcracks can increase the permeability of salt. In this paper, an analytical formulation of the permeability of damaged rock salt is presented for both initially intact and porous conditions. The analysis shows that permeability is related to the connected (i.e., gas accessible) volumetric strain and porosity according to two different power-laws, which may be summed to give the overall behavior of a porous salt with damage. This relationship was incorporated into a constitutive model, known as the Multimechanism Deformation Coupled Fracture (MDCF) model, which has been formulated to describe the inelastic flow behavior of rock salt due to coupled creep, damage, and healing. The extended model was used to calculate the permeability of rock salt from the Waste Isolation Pilot Plant (WIPP) site under conditions where damage evolved with stress over a time period. Permeability changes resulting from both damage development under deviatoric stresses and damage healing under hydrostatic pressures were considered. The calculated results were compared against experimental data from the literature, which indicated that permeability in damaged intact WIPP salt depends on the magnitude of the gas accessible volumetric strain and not on the total volumetric strain. Consequently, the permeability of WIPP salt is significantly affected by the kinetics of crack closure, but shows little dependence on the kinetics of crack removal by sintering.

---

* Work supported by the U. S. Department of Energy (DOE) under Contract No. DE-AC94-AI85000
** A DOE facility
+ Permanent address: Technion, Dept. Mech. Eng., Haifa, Israel

INTRODUCTION

The Waste Isolation Pilot Plant (WIPP) is an underground storage facility located in the salt formations of southeastern New Mexico, which is proposed for use as a permanent repository for transuranic nuclear waste provided it is in compliance with the applicable regulations. Some of the properties that make rock salt attractive as a nuclear waste storage medium include favorable creep characteristics and low gas permeability. It is presumed that creep of salt would encapsulate the waste, while the low gas permeability of salt, coupled with an effective seal system for shafts, would prevent release of the radioactive or hazardous waste to the environment.

Creep of salt, however, can induce the formation of microcracks with time under low confinement conditions. These creep-induced microcracks are located in disturbed rock zones (DRZ) around the underground rooms and in the shafts connected to the underground rooms [1]. The formation of microcracks can accelerate the damage process and affect adversely the structural integrity of the repositories. Furthermore, the microcracks can increase the permeability of salt, thereby reducing the effectiveness of the seal systems and increasing the likelihood of radioactive nuclide release to the environment. Consequently, an accurate prediction of creep-induced damage and the corresponding change in salt permeability is required for assessing the performance of the repositories. The analytical tools necessary for achieving this goal include, among other things, a constitutive model that treats creep, damage, and damage healing in salt and an established functional relationship between permeability and damage.

DISCLAIMER

DISCLAIMER

Portions of this document may be illegible in electronic image products. Images are produced from the best available original document.

Constitutive equations for creep of salt are fairly well established and compare favorably with field measurements. Some of the constitutive models for salt include those formulated by Cristescu [2], Munson and Dawson [3], Aubertin et al. [4-6], Chan et al. [7-14], and Desai and Zhang [15]. Initial, significant steps have also been taken in the simulation of fracture and healing. The constitutive model developed by Chan et al. [7-14], treats coupled creep, fracture, and healing in rock salt. This model was first developed as a set of constitutive equations, referred to as the Multimechanism Deformation (M-D) model, for treating transient and steady-state creep due to dislocation flow mechanisms [3, 16]. Tertiary creep was represented by extending the M-D model to include the evolution of damage during deformation [7, 8]. The extended model, referred to as the Multimechanism Deformation Coupled Fracture (MDCF) model, was formulated by incorporating continuum, isotropic damage as a fully coupled variable that enhances the stress influence by reduction of the effective area and contributes directly to the inelastic strain rate [7-9]. Despite utilizing a scalar damage parameter, the model is capable of indicating the nonisotropic dependence of inelastic straining on the stress state and the confining pressure because the subsidiary equations include the effect of pressure to suppress damage development. Damage healing by a hydrostatic pressure was formulated and incorporated in the latest model development [12-14]. The model, however, did not have a provision for predicting the permeability of rock salt because an explicit relation between permeability and damage had not been developed.

Compacted crushed salt is considered for use as a long-term shaft seal material. In such a seal design, the permeability of the compacted crushed salt in the shaft seal and the permeability of damaged salt in the DRZ near the shaft are important factors which determine, in part, the effectiveness of the seal system. The permeability of intact salt, damaged intact salt, and

compacted crushed salt has been measured in a number of investigations [17-23]. Experimental evidence indicates that the permeability of laboratory test specimens of intact salt generally show large variability because of pre-existing damage in individual specimens [17]. Recent permeability measurements performed on WIPP salt that was predamaged by creep show increased permeability with increasing volumetric strain due to creep damage [20, 23]. Large variations in the permeability of compacted crushed salt were also reported [21, 22]. A comparison of the permeability of damaged intact salt and compacted crushed salt from the WIPP site is presented in Figure 1, which shows a semi-log plot of fractional density versus permeability. The results indicate that the permeability in salt increases with decreasing fractional density. The damaged intact salt exhibits a considerably higher permeability when compared to the compacted crushed salt at equivalent fractional density. Correlation of experimental data from various investigations shows a large variability in the permeability at a given fractional density. Because of the variability, a precise, simple relationship between permeability and fractional density is not initially apparent. The increase in permeability of damaged intact salt over undamaged salt underscores the importance of establishing the proper dependence of permeability on damage.

The objective of this paper is to present a theoretical analysis whose goal is to establish a functional relationship between permeability and damage for WIPP salt. The paper is organized into two parts. In the first, relationships are formulated between permeability and damage in three different types of salt: porous salt, damaged intact salt, and porous salt with damage. The formulations lead to explicit functional relationships between permeability, volumetric strain, and porosity. These relations are compared to experimental laboratory data of WIPP salt from the literature. In the second part of the paper, incorporation of the salt permeability equation into

the MDCF model is described, followed by comparisons of model calculations against experimental results of WIPP salt subjected to either damaging or healing conditions.

MODELING OF SALT PERMEABILITY

Permeability models in the literature can be divided into those of the phenomenological origin [24-26] and those developed based on percolation theory [19, 27-31]. The former models are suitable for porous materials, while the latter models are usually more suitable for materials containing fractures or cracks. A combination of these two approaches has been used to develop a permeability model for porous salt with damage. Figure 2 shows the sequence in which the permeability model has been developed. First, the permeability of porous salt has been considered as a function of porosity, Figure 2(a). Here, the Carman-Kozeny model [24, 25] is applicable and has been used to establish relationships between permeability and porosity. Second, the permeability of intact rock salt with microcracks is treated by focusing on fluid flow through open microcracks, Figure 2(b). In this case the formulation is based on the one proposed by Peach [19], and it leads to a relation between permeability and volumetric strain. Third, the permeability of a porous salt with microcracks is considered, Figure 2(c), by considering the total flow as the sum of those through pores and microcracks, which leads to a nonlinear relationship between permeability, porosity, and volumetric strain due to damage (i.e., opening of microcracks).

(1) Porous Salt

Fluid flow through a porous medium is typically modeled by averaging the microscale interstitial flow velocities associated with the microscale pressure gradient across an assemblage of idealized elementary pores. A well-known model for flow in a porous medium with connected

porosity is that due to Carman and Kozeny [24, 25]. This model can be derived by assuming Hagen-Poiseville flow through a network of tubular pores. The average interstitial flow velocity $\langle v_i \rangle$ is then expressed in terms of the Hagen-Poiseville equation [19, 26]

$$\langle \mathbf{v}_i \rangle = - \frac{D_H^2}{16\theta^* \mu^*} \frac{\Delta P}{L_e} \tag{1}$$

where $\Delta P/L_e$ represents the macroscopic pressure gradient with respect to the average network length, L_e; D_H is the average hydraulic (channel) diameter; μ^* is the fluid viscosity; θ^* is a geometric shape factor. The average interstitial velocity, $\langle v_i \rangle$, is related to the macroscopic velocity, v, according to

$$\langle \mathbf{v}_i \rangle = \frac{\mathbf{v}}{\phi} \left(\frac{L_e}{L} \right) \tag{2}$$

where ϕ is fully connected porosity, and L is the direct macroscopic distance. The ratio of L_e/L represents the tortuosity parameter, T_p, of the flow path. An expression for permeability is then obtained by inserting the macroscopic velocity, v, into Darcy's law for macroscopic flow. According to the Carman-Kozeny model [24, 25], the permeability of a porous salt can be described by [19]

$$K_{CK} = C_{CK} \left[\frac{\phi^3}{(1 - \phi)^2} \right] \tag{3}$$

where K is permeability, C is a constant, and the subscript CK denotes Carman-Kozeny parameters. The Carman-Kozeny constant, C_{CK}, is given by [19]

$$C_{CK} = \frac{1}{\theta^* T_p^2 S_o^2} \tag{4}$$

where T_p is the tortuosity parameter, and S_o is the specific pore surface area. In the present investigation, C_{CK} was treated as a material constant whose value was evaluated from permeability data.

The permeability of compacted crushed WIPP salt was determined earlier by Brodsky et al. [22]. This result, shown in Figure 3, was used to test the validity of the Carman-Kozeny model, Eq. (3). The porosity, ϕ, of crushed salt was taken to be $1 - D_f$, where D_f is the final dry fractional density. The value of C_{CK} was evaluated by fitting Eq. (3) to the experimental data of the permeability of compacted crushed WIPP salt and $C_{CK} = 1 \times 10^{-14}$ m^2 was obtained. The result is compared against experimental data in Figure 3. It is apparent that the calculated curve is representative of these experimental data. Figure 3 shows that the calculated permeability, K_{CK}, decreases rapidly with decreasing porosity and K_{CK} goes to zero as ϕ approaches zero.

(2) Damaged Intact Salt

The permeability of a cracked medium is customarily analyzed by establishing a description of the fluid flow properties of an isotropic assemblage of connected cracks in terms of their average dimensions and number density. The degree of conduction between cracks is then addressed through a statistical treatment of connectivity between randomly placed microcracks in the medium. Such a treatment provides a description of the critical threshold of percolation and the development of conductivity of connected cracks immediately above this threshold. This approach was taken by Peach [19] to obtain post-critical permeability expressions for two

idealized situations of the damage process: (1) growth in the density of microcracks at constant average crack dimensions, and (2) growth in dilatation by crack opening at a constant microcrack density. The permeability of damaged intact salt was treated in terms of Peach's percolation model for the case of constant crack density by assuming that the fluid flow through the connected network of microcracks in salt is solely accommodated by opening of the microcracks. Figure 1(c) shows this configuration. This particular model relates permeability to volumetric strain according to [19]

$$K_P = C_P \left(-\epsilon_{kk}\right)^3 \tag{5}$$

where ϵ_{kk} is the volumetric strain, C_P is a constant, and the subscript P denotes parameters corresponding to the Peach model. The model constant C_P is given by [19]

$$C_P = \frac{\theta \pi^2 <c>^2}{480 \alpha_P} \tag{6}$$

where θ is the hydraulic shape and drag factor, <c> is the mean crack radius, and α_P is a crack shape parameter. The parameter C_P was treated as an empirical constant whose value was evaluated from the permeability data for damaged intact WIPP salt [23], and the value of C_P was determined to be 3×10^{-8} m^2. Comparison of calculated and measured permeability as a function of volumetric strain for damaged intact WIPP salt is shown in Figure 4. The model calculation is an excellent representation of the permeability data because that set of data was used to evaluate the model constant, C_P. The agreement indicates that the power-law relation with an exponent of three in the Peach model, Eq. (5), is essentially correct.

(3) Porous Salt With Damage

The permeability of a porous salt with damage is derived by relating the total macroscopic flow velocity, v, to the macroscopic pressure gradient, $\Delta P/L$, according to [19, 26]

$$v = K\left(\frac{\Delta P}{L}\right) \tag{7}$$

where K is the permeability of the damaged porous medium. The total macroscopic flow velocity is the sum of the flow through cracks, v_{crack}, and pores, v_{pore}, as expressed by

$$v = v_{crack} + v_{pore} \tag{8}$$

with

$$v_{crack} = K_{crack}\left(\frac{\Delta P}{L}\right) \tag{9}$$

$$v_{pore} = K_{pore}\left(\frac{\Delta P}{L}\right) \tag{10}$$

where K_{crack} and K_{pore} are the permeabilities of the cracks and pores, respectively. Eqs. (8), (9), and (10) can be combined with Eq. (7) to obtain

$$K = K_P + K_{CK} \tag{11}$$

when the permeability of the pores and cracks are represented by the Carman-Kozeny and the Peach models, respectively. Upon substituting Eqs. (3) and (5) into (11), the permeability for a damaged porous material is obtained as

$$K = C_p(-\epsilon_{kk})^3 + C_{CK}\,\phi^3\,(1-\phi)^{-2} \tag{12}$$

where the first term in the right hand side treats the microcracks, and the second term treats the porosity. If D_f is the fractional density of the damaged porous material, then

$$1 - D_f = \phi - \epsilon_{kk} \tag{13}$$

since both the porosity, ϕ, and the volume strain, ϵ_{kk}, due to damage contribute to the density change. If one defines γ as the ratio given by

$$\gamma = \frac{\phi}{\phi - \epsilon_{kk}} \tag{14}$$

then

$$1 - \gamma = \frac{-\epsilon_{kk}}{\phi - \epsilon_{kk}} \tag{15}$$

which may be combined with Eqs. (12) and (13), leading to

$$K = (1 - \gamma)^3 C_p (1 - D_f)^3 + \left[\frac{\gamma^3 D_f^2}{(1 - \gamma + D_f)^2}\right] C_{CK} (1 - D_f)^3 D_f^{-2} \qquad (16)$$

as the permeability for a damaged porous medium. Eq. (16) reduces to the Carman-Kozeny relation when $\gamma = 1$, but gives the Peach relation when $\gamma = 0$. Figure 5 shows the permeability, K, as a function of the fractional density, D_f, for various values of the γ parameter. From Figure 5 it is clear that the permeability at a given fractional density increases rapidly with decreasing values of the γ parameter because the contribution of volumetric strain to permeability increases with $1 - \gamma$. Permeability is also more sensitive to the volumetric strain than to the porosity because the value of C_P is several orders of magnitude higher than C_{CK}. As a consequence, the presence of a small volumetric strain due to damage causes a relatively large increase in the permeability of a porous material. For example, the permeability of a porous salt with a fractional density of 0.95 is increased by two orders of magnitude over that of the Carman-Kozeny model if 5% of the density change is due to the volumetric strain associated with damage (i.e., $1 - \gamma = 0.05$) and the remaining density change arises from porosity ($\gamma = 0.95$).

A comparison of model calculations and experimental results of permeability of WIPP salt as a function of fractional density is presented in Figure 5. For a given fractional density, the Carman-Kozeny model is in agreement with the brine permeability data from Brodsky et al. [22], while the Peach model is in agreement with the experimental data of damaged intact salt from Pfeifle [23]. The lower bound of measured permeability is delineated by the Carman-Kozeny model, and the upper bound is delineated by the Peach model. All other permeability data [18, 20, 21] lie between these two bounds and can be described by γ values of 0.75 and 0.95. The implications of the results shown in Figure 5 are that (1) the permeability of compacted

crushed WIPP salt in the experiment of Brodsky et al. [22] was controlled by the porosity in the salt; (2) the permeability in damaged intact salt in Pfeifle's experiment [23] was controlled by microcracks in the salt; (3) the permeability attributed to microcracks was much greater than that attributed to porosity; (4) the intermediate levels of permeability observed in other conditions may be explained on the basis of the presence of small amounts (5-25%) of crack-like defects in the material that behaved like microcracks as far as permeability is concerned.

The developments given above have some very important implications in treating permeability. Since the effect of damage on permeability is several orders of magnitude stronger than that due to porosity, volumetric strain due to damage and porosity cannot be mixed when the permeability of a damaged porous salt is considered. Even though the contributions of porosity and volume strain (due to damage) to density change are linearly additive, Eq. (13), their effects on permeability cannot be obtained by summing porosity and volume strain as an effective porosity and using the Carman-Kozeny model, Eq. (3). Instead, Eq. (12) or (16) must be used.

INCORPORATING PERMEABILITY FUNCTION INTO THE MDCF MODEL

In this section, the permeability model is incorporated into the MDCF constitutive model for the case of damaged intact salt. As a result, only the incorporation of the Peach relation into the MDCF model is considered. In the MDCF formulation [1, 2, 14], the total strain rate, $\dot{\epsilon}_{ij}^{t}$, for a solid deformed under isothermal conditions is given as the sum of the elastic strain rate, $\dot{\epsilon}_{ij}^{e}$, and the inelastic strain rate, $\dot{\epsilon}_{ij}^{I}$. The inelastic strain rate is further decomposed into four components corresponding to contributions from dislocation creep, shear damage, tensile damage, and damage healing. The overall flow law is described in terms of a generalized kinetic equation [32] that contains the creep, damage, and healing terms, as given by [14]

$$\dot{\varepsilon}^{I}_{ij} = \frac{\partial \sigma^{c}_{eq}}{\partial \sigma_{ij}} \dot{\varepsilon}^{c}_{eq} + \frac{\partial \sigma^{\omega_s}_{eq}}{\partial \sigma_{ij}} \dot{\varepsilon}^{\omega_s}_{eq} + \frac{\partial \sigma^{\omega_t}_{eq}}{\partial \sigma_{ij}} \dot{\varepsilon}^{\omega_t}_{eq} + \frac{\partial \sigma^{h}_{eq}}{\partial \sigma_{ij}} \dot{\varepsilon}^{h}_{eq} \tag{17}$$

where σ^{c}_{eq}, $\sigma^{\omega_s}_{eq}$, $\sigma^{\omega_t}_{eq}$, σ^{h}_{eq} are the power conjugate equivalent stress measures for dislocation creep, shear damage, tensile damage, and damage healing, respectively. The corresponding effective strain rate measures are $\dot{\varepsilon}^{c}_{eq}$, $\dot{\varepsilon}^{\omega_s}_{eq}$, $\dot{\varepsilon}^{\omega_t}_{eq}$, and $\dot{\varepsilon}^{h}_{eq}$. In Eq. (17), the conjugate equivalent stress plays the role of a flow potential for individual deformation mechanisms, and the derivative with stress gives the direction of inelastic strain rate. The magnitude of the inelastic strain rate is given by the kinetic equation that relates the equivalent strain rate to the corresponding power-conjugate equivalent stress measure and the internal variables representing the current states of deformation and damage. A summary of the conjugate equivalent stress and strain rate measures for individual deformation mechanisms is presented next.

(1) Conjugate Equivalent Stress Measures

Inelastic flow due to dislocation creep is isochoric and pressure-independent. These features lead to a conjugate equivalent stress measure for dislocation creep, σ^{c}_{eq}, which is formulated based on the stress difference as given by [3, 16]

$$\sigma^{c}_{eq} = |\sigma_1 - \sigma_3| \tag{18}$$

where σ_1 and σ_3 are the maximum and minimum principal stresses, with compression being positive. The Tresca equivalent stress measure is preferred over that of von Mises because experimental measurements of the flow surface and inelastic strain rate vector are in better agreement with the Tresca formulation [16].

Damage development in compression is considered to arise from microcrack sliding due to shear and the opening of wing-tip cleavage cracks that develop on some of the shear cracks. The resulting inelastic flow includes deviatoric and dilatational components which are pressure dependent. These characteristics have been accounted for in a nonassociated flow formulation by using two conjugate equivalent stress measures, one for the flow law and another for the kinetic equation. These stress measures are [7, 8, 14]

$$\left[\sigma_{eq}^{\omega_s}\right]_f = |\sigma_1 - \sigma_3| - x_2 x_8 [I_1 - \sigma_1]/3 \tag{19}$$

for the flow law and

$$\left[\sigma_{eq}^{\omega_s}\right]_k = |\sigma_1 - \sigma_3| - x_2 x_7 sgn(I_1 - \sigma_1)\left[\frac{I_1 - \sigma_1}{3x_7 sgn(I_1 - \sigma_1)}\right]^{x_6} \tag{20}$$

for the kinetic equation; where I_1 is the first invariant of Cauchy stress; the x_i's are material constants; sgn( ) is the signum function. The first terms on the right-hand side of Eqs. (19) and (20) represent shear-induced damage, which manifests as slip-induced shear microcracks. Some of these microcracks develop wing tips that generate inelastic strains that add to those originating from dislocation flow mechanisms. Opening of these wing cracks, which are aligned parallel to the maximum principal stress (σ_1), occurs in directions normal to the σ_1 direction and is resisted by compressive stresses of σ_2 and σ_3. The second terms in the right-hand side of Eqs. (19) and (20), which are in the form of f($I_1 - \sigma_1$), model the effects of stress state on aiding or suppressing the opening of wing cracks.

Tensile creep damage in salt occurs in the form of cleavage microcracks aligned normal to the tensile stress. The kinetics of tensile damage in salt is substantially faster than shear damage

and is therefore treated as a separate term. The conjugate equivalent stress measure for tensile damage-induced flow is [11]

$$\sigma_{eq}^{\omega_t} = -x_1 \sigma_3 H(-\sigma_3) \tag{21}$$

where H( ) denotes the Heaviside step function. This stress measure is intended to represent the opening of microcracks by a tensile stress, σ_3.

Reduction of damage in rock salt can occur by the closure of open microcracks and the sintering of microcracks. Both processes can be considered to be driven by an identical thermodynamic driving force represented by a pertinent power-conjugate equivalent stress measure. If the healing process is isotropic, the appropriate power-conjugate equivalent stress measure would be the first invariant, I_1, of the Cauchy stress. On the other hand, damage healing might be nonisotropic or exhibit induced anisotropy. For this situation, a second stress term in addition to I_1 is required. For describing stress-induced healing anisotropy, the conjugate equivalent stress measure for damage healing may be taken as [12, 13, 14]

$$\sigma_{eq}^{h} = \frac{1}{3}(I_1 - x_{10}\sigma_1) \tag{22}$$

where x_{10} is a material constant. One of the characteristics of this conjugate equivalent stress measure is that when used in conjunction with Eq. (17), the healing term is the only nonzero term under hydrostatic compression. In addition, healing may also occur under nonhydrostatic compression.

(2) Equivalent Strain Rate Measures

The kinetic equation representing the creep rate, $\dot{\epsilon}^{c}_{eq}$, due to dislocation flow mechanisms was formulated by Munson and Dawson [3] and is given by

$$\dot{\epsilon}^{c}_{eq} = F \sum_{i=1}^{3} \dot{\epsilon}_{s_i} \tag{23}$$

where F is the transient function representing transient creep behavior, and $\dot{\epsilon}_{s_i}$ is the steady-state strain rate for the i^{th} independent dislocation flow mechanism. The mechanisms include dislocation climb (i = 1), dislocation glide (i =3), and one that has not been identified mechanistically, but which is fully characterized experimentally (i = 2). The steady-state strain rates are [3]

$$\dot{\epsilon}_{s_i} = A_i e^{-Q_i/RT} \left[\frac{\sigma^{c}_{eq}}{\mu(1 - \omega)} \right]^{n_i} \tag{24}$$

for i = 1, and 2, and

$$\dot{\epsilon}_{s_3} = |H| \left(\sum_{i=1}^{2} B_i e^{-Q_i/RT} \right) \sinh\left[\frac{q}{\mu} \left(\frac{\sigma^{c}_{eq}}{1 - \omega} - \sigma_o \right) \right] \tag{25}$$

for i = 3, where the A_i's and B_i's are constants, Q_i's are activation energies, T is absolute temperature, R is the universal gas constant, μ is shear modulus, n_i's are the stress exponents, q is the stress constant, H is the Heaviside function with $[\sigma^{c}_{eq}/(1-\omega) - \sigma_o]$ as the argument, σ_o is the stress limit of the dislocation glide mechanism, and ω is the Kachanov [33] isotropic damage variable.

The kinetic equation of damage-induced inelastic flow was developed on the basis that wing cracks developed at the tips of sliding shear cracks or slipbands. As a result, the kinetic equation for shear-induced damage followed closely to that for dislocation glide. The same form of expression was also used for the kinetic equation for tensile damage-induced flow and is given by [8, 10, 11]

$$\dot{\epsilon}_{eq}^{\omega_i} = F^{\omega_i} \dot{\epsilon}_s^{\omega_i} \tag{26}$$

where i = s or t for shear or tensile damage, respectively; F^{ω_i} is the transient function for the i^{th} mode of damage. The kinetic equations for damage-induced flow, $\dot{\epsilon}_s^{\omega_i}$, during steady-state creep are expressed by

$$\dot{\epsilon}_s^{\omega_i} = c_o \left(\sum_{i=1}^{2} B_i e^{-Q_i/RT} \right) \omega_o e^{c_3 \omega} \left[\sinh \left(\frac{c_2 \sigma_{eq}^{\omega_i} H(\sigma_{eq}^{\omega_i})}{(1-\omega)\mu} \right) \right]^{n_3} \tag{27}$$

where c_i's and n_3 are material constants, and ω_o is the initial value of the damage variable, ω. The kinetic equation in Eq. (27) allows $\dot{\epsilon}_{eq}^{\omega_i}$ to exhibit a transient behavior by virtue of the transient function, F^{ω_i}, which is directly related to the transient function, F, for creep. The expressions for the transient functions can be found in earlier publications [8, 10, 11].

Experimental evidence indicated that two healing mechanisms might be present in WIPP salt. Each of the two healing mechanisms may be described by a first-order kinetic equation. The first mechanism, which is closure of microcracks, has a smaller time constant, τ_1, than the time constant, τ_2, for the second mechanism, which is healing of microcracks. The kinetic equation for damage healing in WIPP salt is taken to be [13, 14]

$$\dot{\epsilon}^{h}_{eq} = \frac{\epsilon_{kk}\left(\sigma^{h}_{eq} - \sigma_b\right) H\left(\sigma^{h}_{eq} - \sigma_b\right)}{\tau \mu} \tag{28}$$

with

$$\sigma_b = x_7 \left| \frac{\sigma_1 - \sigma_3}{x_2 x_7} \right|^{\frac{1}{x_6}} \tag{29}$$

where ϵ_{kk} is the volumetric strain, H ( ) is the Heaviside function with its argument in parenthesis, and τ is the characteristic time for damage healing. The parameter σ_b, which represents the stress threshold for healing, is assumed to coincide with the dilatancy boundary and is obtained by setting $\sigma^{\omega}_{eq} = 0$ in Eq. (20) [11] and by using $\sigma_b = \frac{1}{3}(I_1 - \sigma_1)$. The expression for σ^{h}_{eq} is given in Eq. (22), which indicates that σ^{h}_{eq} depends on the parameter x_{10}. Earlier work has established that damage healing in WIPP salt occurs by two different healing mechanisms (crack closure and sintering) with different characterisitic times, degrees of healing anisotropy, and x_{10} values [13]. Based on the strain anisotropy observed during damage healing, the value of x_{10} was taken to be 1.14 in the flow law, which is the average of the x_{10} values for the healing mechanisms. On the other hand, the value of x_{10} was taken to be 1.0 in the kinetic equation, which is the x_{10} value determined for healing by crack sintering. This choice of the x_{10} value was also motivated by the consideration of the damage and healing boundaries in the stress space. The damage and healing boundaries coincide when $x_{10} = 1$. In general, damage healing tends to reduce ϵ_{kk} to zero. To account for two characteristic times, τ is taken to be a function of the volumetric strain according to the relation given by [13, 14]

$$\tau = \tau_0 \exp\left(k_1 \epsilon_{kk}\right) + \tau_1 \quad for \quad \epsilon_{kk} < 0 \tag{30}$$

where k_1 is a material constant, and τ_0 and τ_1 are characteristic time constants. Additionally,

$$\tau = \tau_0 + \tau_1 \quad for \quad \varepsilon_{kk} < 0 \tag{31}$$

According to Eq. (30), the characteristic time, τ, takes on a limiting value of τ_1 when the volumetric strain has a large negative value and the exponential term becomes zero. This characteristic time corresponds to damage healing by closure of microcracks. When the volumetric strain is small (small negative value), the value of the characteristic time, τ, is increased from τ_1 to a larger value that approaches $\tau_0 + \tau_1$, which corresponds to the characteristic time constant for crack sintering or removal.

(3) Damage Evolution Equations

An internal variable in the context of Kachanov's isotropic damage parameter [33], ω, was used as a measure of current damage in the deformed solid. Damage development in the MDCF model is described in terms of an evolution equation that contains both damage growth and healing terms, as given by [12-14]

$$\dot{\omega} = g(\omega, T, \sigma_{eq}^{\omega_i}, \chi_i) - h(\omega, T, \sigma_{eq}^{h}) \tag{32}$$

where $g(\omega, T, \sigma_{eq}^{\omega_i}, \chi_i)$ describes the growth of damage, and $h(\omega, T, \sigma_{eq}^{h})$ describes the healing of damage. The damage growth function, g, is given by [8, 11]

$$g = \frac{x_4}{t_o}\omega\left[\ln\left(\frac{1}{\omega}\right)\right]^{\frac{x_4+1}{x_4}}\left\{\left[\frac{\sigma_{eq}^{\omega_s} H(\sigma_{eq}^{\omega_s})}{\chi_s}\right]^{x_{3s}} + \left[\frac{\sigma_{eq}^{\omega_t} H(\sigma_{eq}^{\omega_t})}{\chi_t}\right]^{x_{3t}}\right\} \tag{33}$$

where x_{3i}, x_4, χ_i (with i = s or t for shear or tensile damage, respectively) are material constants, and t_o is a reference time. Motivated by the experimental observations [34] the healing function is taken to be a first-order kinetic equation given by [13, 14]

$$h = \frac{\omega \left(\sigma^{h}_{eq} - \sigma_b\right) H\left(\sigma^{h}_{eq} - \sigma_b\right)}{\tau \mu} \tag{34}$$

which has the same form as the kinetic equation for damage healing, Eq. (28) and $x_{10} = 1$ in the calculation of σ^{h}_{eq}, Eq. (22). The overall evolution equation for damage with healing is obtained by combining Eq. (32) with Eqs. (33) and (34).

(4) Permeability and Volumetric Strains

The coupling between permeability and damage is through the volumetric strain term. It is envisioned that the volumetric strain resulting from damage would increase permeability by providing a gas accessible path. During damage healing, the volumetric strain is reduced first by crack closure and then by crack sintering. Closure of cracks is expected to vary along the gas path and result in local blockages. Once blocked, the gas path becomes inaccessible and less permeable. In this circumstance, the important parameter that controls permeability is the gas accessible volumetric strain. Because of this, the Peach relation is incorporated into the MDCF model as

$$K_P = C_P(-\epsilon^{g}_{kk})^3 \tag{35}$$

where ϵ^{g}_{kk} is the gas accessible (i.e., connected) volumetric strain which is obtained by integrating the volumetric strain rate over time, as given by

$$\epsilon^{g}_{kk} = \int (\dot{\epsilon}^{e}_{kk} + \dot{\epsilon}^{\omega_s}_{kk} + \dot{\epsilon}^{\omega_t}_{kk} + \dot{\epsilon}^{g}_{kk})\, dt \tag{36}$$

where $\dot{\epsilon}^{e}_{kk}$ is the elastic volume strain rate, and $\dot{\epsilon}^{\omega_s}_{kk}$, $\dot{\epsilon}^{\omega_t}_{kk}$, and $\dot{\epsilon}^{g}_{kk}$ are the inelastic volumetric strain rates due to shear damage, tensile damage, and healing by crack closure, respectively. The last term is given by

$$\dot{\epsilon}^{g}_{kk} = \dot{\epsilon}^{h}_{eq} = \frac{\epsilon^{g}_{kk} (\sigma^{h}_{eq} - \sigma_b)\, H(\sigma^{h}_{eq} - \sigma_b)}{\tau \mu} \tag{37}$$

which is obtained from Eq. (28) by replacing the actual volumetric strain, ϵ_{kk}, by the connected (gas accessible) volumetric strain, ϵ^{g}_{kk}. It is noted that the gas accessible volumetric strain would decrease by the crack closure healing mechanism but is not significantly influenced by the sintering mechanism. Therefore, the characteristic time, τ, in Eq. (37) would be essentially τ_1 but is also considered to vary with the stress state such that τ is given by Eq. (30) for $\sigma^{h}_{eq} \leq \sigma_{th}$, but $\tau = \tau_1$ for $\sigma^{h}_{eq} > \sigma_{th}$, where σ_{th} is the hydrostatic pressure below which the characteristic time changes from τ_1 to τ. As discussed later, $\sigma_{th} = 3.5$ MPa for WIPP salt.

EVALUATION OF MODEL CALCULATIONS AGAINST EXPERIMENTAL RESULTS

(a) During Damage Healing

Stormont [20, 35] had reported the permeability of WIPP salt that was initially damaged and then subjected to healing under hydrostatic pressure. Measurements of permeability were determined as a function of time for hydrostatic healing pressures initially at about 2.41 MPa. The hydrostatic pressure was then increased up to 14.48 MPa. Results for several specimens were reported. These results were used to compare with the permeability calculated using the MDCF model. The same loading history was used in the MDCF model simulation calculations. To simulate identical initial damage, triaxial creep was used in the initial part of the model calculation to generate a damage condition that gave the same permeability as observed in the experiment. Subsequently, the hydrostatic pressure was imposed according to those used in the experiment. The model constants used in these calculations are shown in Tables 1 and 2.

In the tests conducted on specimens TUA9 and TUA6, permeability was measured initially at a hydrostatic pressure of 2.41 MPa, which was subsequently increased to 14.48 MPa. Permeability was then measured as a function of time. Comparison of the calculated and measured values of permeability for specimens TUA9 and TUA6 is shown as a function of confining pressure in Figure 6, which indicates that the decrease in permeability with increasing hydrostatic pressures is accurately predicted by the model. The corresponding results of permeability as a function of time of healing are shown in Figure 7. Permeability measurements for nine other specimens reported by Stormont [20] are also included in Figure 7. The very short time response (less than 1 hour) in Figure 7 perhaps indicates that the actual response is not linear as the model would suggest. However, the model does predict something of an average behavior for the other ten specimens.

The results in Figure 7 indicate that reduction of permeability occurs fairly rapidly with time when the hydrostatic pressure was 14.48 MPa. This finding was consistent with the small value of the characteristic time of crack closure. The implication is that permeability reduction in WIPP salt is controlled by closure and not by sintering of microcracks. Such a finding is consistent with the prevailing view that a continuous, gas accessible path is required for achieving a high permeability [19, 20, 24-31, 35]. Conversely, a blocked path is all that is required for attaining a low permeability. Since the characteristic time for crack closure is very small, the kinetics of permeability reduction is consequently fairly rapid.

The calculation involved damage healing of specimen TUA10 at a hydrostatic pressure of 2.41 MPa is presented in Figure 8, which shows comparison of the calculated and measured values of permeability as a function of time of healing. Figure 8 indicates that at 2.41 MPa pressure the permeability of WIPP salt does not vary significantly with time, at least for the time period considered. This experimental observation is consistent with the need for using two different characteristic healing times depending upon whether the applied hydrostatic pressure is below or above 3.5 MPa.

(b) During Damage Generation

After hydrostatic healing, Stormont deformed the WIPP salt specimens under triaxial compression at an approximately constant rate in the range of 1×10^{-6} to 3×10^{-5} sec^{-1} [20]. Permeability was then measured at various strain levels under strain hold conditions. These experiments were conducted at confining pressures of 2.41, 4.14, 5.86, and 7.59 MPa. The MDCF model was used again in these permeability calculations. The calculated and measured values of permeability are presented in Figures 9 and 10 for the case of triaxial compression

under confining pressures of 2.41 and 7.59 MPa, respectively. The permeability for undamaged salt is generally reported to be about $1 \times 10^{-21} m^2$, [20], which is shown as dashed lines in Figures 9 and 10. This permeability value for undamaged salt should be considered an approximate value since experimental determination of such a low permeability is difficult and might be limited by the sensitivity of the instrumentation. With this limitation in mind, Figures 9 and 10 indicate that the permeability of salt damaged during triaxial compression is considerably higher than that of the undamaged salt. The agreement between model calculations and experimental data is within an order of magnitude in permeability for the case of triaxial compression under 2.41 MPa confining pressures, as shown in Figure 9. On the other hand, Figure 10 shows that there is some discrepancy between the calculation and the experimental data for triaxial compression under 7.59 MPa confining pressure. The calculated permeability was substantially lower than the experimental data for strain levels less than 0.05, as shown in Figure 10. The lower permeability in the calculation was the result of damage suppression by a relatively high confining pressure (7.58 MPa). However, the permeability data of Stormont did not show such a pressure effect. To understand this discrepancy between model and experiment, the calculated and measured inelastic volumetric strains for individual specimens are compared in Figures 11 and 12. The comparison indicates that the calculated and measured inelastic volumetric strains were in agreement (to the degree of within experimental scatter) for triaxial compression under a confining pressure of 2.41 MPa, as shown in Figure 11. In contrast, Figure 12 shows that for triaxial compression at 7.59 MPa confining pressure, the calculated volumetric strain is in agreement with that for TUA15 and to a lesser extent with specimen TUA9. The predicted volumetric strain is considerably less than that observed in specimen TUA16. In TUA9, the inelastic volumetric strain was essentially zero at axial strains less than 0.07. The reported permeability for this region was in the range of 1×10^{-19} to 1×10^{-20} m^2,

which appeared to be quite high for zero volumetric strain. It is probable that this discrepancy is the result of the normal inability of the experimental apparatus to measure permeabilities below some level of detectability. As a result the high values of permeability reported are not actual permeability, and will not correspond to the calculated values.

CONCLUSIONS

An analytical treatment of permeability in porous salt with damage was formulated to establish a functional relationship between permeability, porosity, and damage. It is shown that the volumetric strain is an appropriate measure of damage in salt, but porosity should not be mixed with the volumetric strain in considering permeability because volumetric strain due to damage exerts a greater effect on permeability than does porosity. An analytical relationship between permeability, porosity, and volumetric strain due to damage was obtained and incorporated into the MDCF constitutive model. The model was used to calculate the permeability of WIPP salt subjected to either damaging or healing conditions. The dependence of permeability on hydrostatic pressure, time of healing, and gas accessible volumetric strain was predicted within reasonable correctness, although discrepancies still exist. Comparisons of model calculations against experimental data from the literature also indicated that the permeability of WIPP salt was primarily controlled by the kinetics of crack closure. The proposed methods show some promise as a predicted tool but its accuracy remains to be tested against field data, which was not possible in this paper.

ACKNOWLEDGEMENTS

The clerical and editorial assistance of Ms. Patty A. Soriano and Ms. Deborah J. Stowitts of Southwest Research Institute are appreciated.

REFERENCES

1. Munson D. E, Holcomb D. J., DeVries K. L., Brodsky N. S., and Chan K. S. Correlation of theoretical calculations and experimental measurements of damage around a shaft in salt, *Proceedings of 35th U. S. Symposium on Rock Mechanics* (edited by Daemen J. J. K. and Schultz R.. A.) pp. 491-496, Balkema, Brookfield VT (1995).

2. Cristescu N. A general constitutive equation for transient and stationary creep of rock salt, *Int. J. Rock Mech. Min. Sci. & Geomech. Abstr.*, 30, pp. 125-140 (1993).

3. Munson D. E. and Dawson P. R. Salt constitutive modeling using mechanism maps, *Proc. First Conf. on the Mechanical Behavior of Salt*, Trans. Tech. Publications, pp. 717-737, Karl Distributors, Rockport MA (1984).

4. Aubertin M., Gill D. E., and Ladanyi B. A unified viscoplastic model for the inelastic flow of alkali halides, *Mech. of Mat.*, 11, pp. 63-82 (1991).

5. Aubertin M., Sgaoula J., and Gill D. E. A damage model for rocksalt: application to tertiary creep, *7th Symposium on Salt*, (edited by Kakihana H., Hardy H. R. Jr., Hoshi T., and Toyokura K.) 1, pp. 117-125, Elsevier Science Publications, New York NY (1993).

6. Aubertin M., Gill D. E., and Ladanyi B. Modeling the transient inelastic flow of rocksalt, *Seventh Symp. on Salt* (edited by Kakihana H., Hardy H. R. Jr., Hoshi T., and Toyokura K.) 1, pp. 93-104, Elsevier Science Publ., New York NY (1993).

7. Chan K. S., Bodner S. R., Fossum A. F., and Munson D. E. A constitutive model for inelastic flow and damage evolution in solids under triaxial compression, *Mech. Mat.*, 14, pp. 1-14 (1992).

8. Chan K. S., Brodsky N. S., Fossum A. F., Bodner S. R., and Munson D. E. Damage-induced nonassociated inelastic flow in rock salt, *Int. J. of Plasticity*, 10, pp. 623-642 (1994).

9. Chan K. S., DeVries K. L., Bodner S. R., Fossum A. F., and Munson D. E. A damage mechanics approach to life prediction for a salt structure, *Computational Mechanics '95*, (edited by Atluri S. N., Yagawa G., and Cruse T. A.) 1, pp. 1140-11145, Springer-Verlag, Berlin (1995).

10. Chan K. S., Munson D. E., Fossum A. F., and Bodner S. R., Inelastic flow behavior of argillaceous salt, *Int. J. Damage Mechanics*, 5, pp. 292-314 (1996).

11. Chan K. S., Bodner S. R., Fossum A. F., and Munson D. E. A damage mechanics treatment of creep failure in rock salt, *Int. J. of Damage Mechanics*, in press (1996). Also available as *SAND93-3902* (under a different title), Sandia National Laboratories, Albuquerque NM (1993).

12. Chan K. S., Bodner S. R., Fossum A. F., and Munson D. E. Constitutive representation of damage healing in WIPP salt, *Proceedings of the 35th U. S. Symposium on Rock*

Mechanics, (edited by Daemen J. J. K. and Schultz R. A.) pp. 485-490, Balkema, Brookfield VT (1995).

13. Chan K. S., Munson D. E., and Bodner S. R. Recovery and healing of damage in WIPP salt, *International Journal of Damage Mechanics*, in press (1996). Also available as *SAND96-0724J*, Sandia National Laboratories, Albuquerque NM (1996).

14. Chan K. S., Munson D. E., Fossum A. F., and Bodner S. R. A constitutive model for representing coupled creep, fracture, and healing in rock salt, *Proceedings of Fourth Conference on the Mechanical Behavior of Salt*, École Polytechnique de Montréal, University of Montréal, June 17-18, 1996, Trans Tech Publication, Karl Distributors, Rockport MA, in press (1996). Also available as *SAND96-0376C*, Sandia National Laboratories, Albuquerque NM (1996).

15. Desai C. S. and Zhang D. Viscoplastic model for geologic materials with generalized flow rule, *Int. J. for Num. & Analy. Methods in Geomechanics*, 11, pp. 603-620 (1987).

16. Munson D. E., Fossum A. F., and Senseny P. E. Advances in resolution of discrepancies between predicted and measured in-situ WIPP room closures, *SAND88-2948*, Sandia National Laboratories, Albuquerque NM (1989).

17. Sutherland H. J. and Cave S. P. Argon gas permeability of New Mexico rock salt under hydrostatic compression, *Int. J. Rock Mech. Min. Sci. Geomech. Abstr.*, 17, pp. 281-288 (1980).

18. Butcher B. M., Novak C. F., and Jercinovic M. The advantages of a salt/bentonite backfill for Waste Isolation Pilot Plant disposal rooms, *SAND90-3074*, Sandia National Laboratories, Albuquerque NM (1991).

19. Peach C. J. Influence of deformation on the fluid transport properties of salt rocks, Ph.D. Thesis, Department of Geology, University of Utrecht, Netherlands (1991).

20. Stormont J. C. Gas permeability changes in rock salt during deformation, Ph.D. Thesis, University of Arizona, Tucson AZ (1990).

21. Brodsky N. S. Hydrostatic and shear consolidation tests with permeability measurements on Waste Isolation Pilot Plant crushed salt, *SAND93-7058*, Sandia National Laboratories, Albuquerque NM (1993).

22. Brodsky N. S., Zeuch D. H., and Holcomb D. J. Consolidation and permeability of crushed WIPP salt in hydrostatic and triaxial compression, *Proceedings of 35th U. S. Symposium on Rock Mechanics* (edited by Daemen J. J. K. and Schultz R. A.) pp. 497-502, Balkema, Brookfield VT (1995).

23. Pfeifle T. W. RE/SPEC Inc., Rapid City, SD 57709, personal communication (1996).

24. Carman P. C. Fluid flow through granular beds, *Trans. Inst. Chem. Eng. London*, 15, pp. 150-166 (1937).

25. Kozeny J. Royal Academy of Science, Vienna, *Proc. Class I.*, 136, 271 (1927). See also reference 26.

26. Dullien F. A. L. *Porous media-fluid transport and pore structure*, Academic Press, New York NY (1979).

27. Dienes J. K. Permeability, percolation and statistical crack mechanics, *Issues in Rock Mechanics*, 23rd Symposium on Rock Mechanics (edited by Goodman R. E. and Heuze F. E.) AIME, New York NY, Ch. 9, pp. 86-94 (1982).

28. Gueguen Y. and Dienes J. Transport properties of rocks from statistics and percolation, *Mathematical Geology*, 21, pp. 1-13 (1989).

29. Englman R., Gur Y., and Jaeger Z. Fluid flow through a crack network in rocks, *J. Appl. Mech.*, 50, pp. 707-711 (1983).

30. Long J. C. S. and Witherspoon P. A. The relationship of the degree of interconnection to permeability in fracture networks, *J. Geo. Res.*, 90, pp. 3087-3098 (1985).

31. Hestir K. and Long J. C. S. Analytical expressions for the permeability of random two-dimensional Poisson fracture networks based on regular lattice percolation and equivalent media theories, *J. Geophys. Res.*, 95, pp. 21565-21581 (1990).

32. Fossum A. F., Callahan G. D., Van Sambeek L. L., and Senseny P. How should one-dimensional laboratory equations be cast into three-dimensional form? *Proceedings of 29th U. S. Symposium on Rock Mechanics* (edited by Cundall P. A., Sterling R. L., and Starfield A. M.) pp. 35-41, Balkema, Brookfield VT (1988).

33. Kachanov L. M. On creep rupture time, *Izv. Akad. Nauk SSSR. Tekh., Nauk: Otdgel.*, 8, pp. 26-31 (1958) (in Russian). See also Kachanov L. M. Introduction to Continuum Damage Mechanics, Martinus Nijhoff Publishers, Boston MA (1986).

34. Brodsky N. S. and Munson D. E. Thermomechanical damage recovery parameters for rocksalt from the Waste Isolation Pilot Plant, *Proceedings of the First North American Rock Mechanics Symposium* (edited by Nelson P. P. and Laubach S. E.) pp. 731-738, Balkema, Brookfield VT (1994).

35. Stormont J. C. and Daemen J. J. K. Laboratory study of gas permeability changes in rock salt during deformation, *Int. J. Rock Mech. Min. Sci. & Geomech. Abstr.*, 29, pp. 325-342 (1992).

Table 1. Material Constants for WIPP Clean Salt

Elastic Properties

μ	12.4 GPa
E	31.0 GPa
ν	0.25

	M-D Model Constants	Damage Model Constants
A_1 (sec^{-1})	8.386 E22	$x_1 = 6$
Q_1 (J/mol)	1.045×10^5	$x_2 = 9$
n_1	5.5	$x_{3s} = 5.5$
B_1 (sec^{-1})	6.086 E6	$x_{3t} = 40$
A_2 (sec^{-1})	9.672 E12	$x_4 = 3$
Q_2 (J/mol)	4.18×10^4	ξ_s= 231.0 MPa for $\sigma > \sigma_o$
n_2	5.0	ξ_s = 351.1 MPa for $\sigma \leq \sigma_o$
B_2 (sec^{-1})	3.03 E-2	ξ_t = 15.15 MPa
σ_o (MPa)	20.57	$x_6 = 0.75$
q	5.335 E3	x_7 = 1 MPa
R (J/mol °K)	8.3143	$x_8 = 0.1$
m	3.0	$c_0 = 5 \times 10^4$
K_o	6.275 E5	$c_2 = 850$
c (K^{-1})	0.009198	$c_3 = 10$
α	-17.37	$c_4 = 6$
β	-7.738	c_5 = 25 MPa
δ	0.58	t_o = 1 sec
		$n_3 = 3$
		$\omega_o = 1 \times 10^4$
		p_1 = 28 (linear approximation)

Table 2. Material Constants in the Damage Healing Model for WIPP Clean Salt

Parameter (Unit)	Temperature		
	20°C	46°C	70°C
τ_o (sec)	2.326×10^5	1.628×10^4	697.7
τ_1 (sec)	11.628	11.628	11.628
k_1	5000	4000	1500
x_{10} (flow law)	1.14	1.14	1.14
x_{10} (kinetic equation)	1.0	1.0	1.0
σ_{th} (MPa)	3.5	—	—

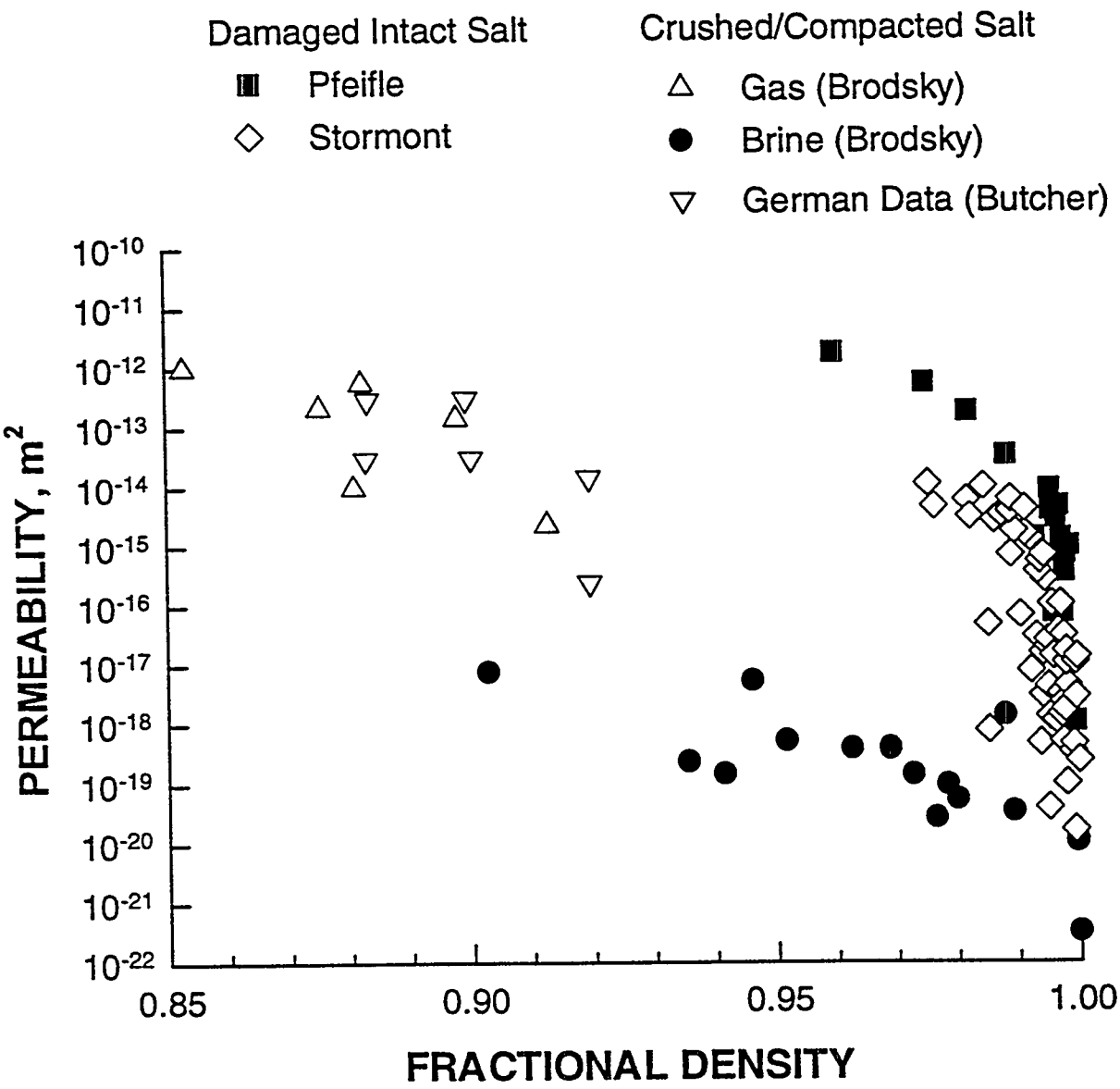

Figure 1. Summary of measured values of permeability in damaged intact salt (Stormont [20], Pfeifle [23]) and compacted crushed salt (Butcher et al. [18], Brodsky [21], Brodsky et al. [22]).

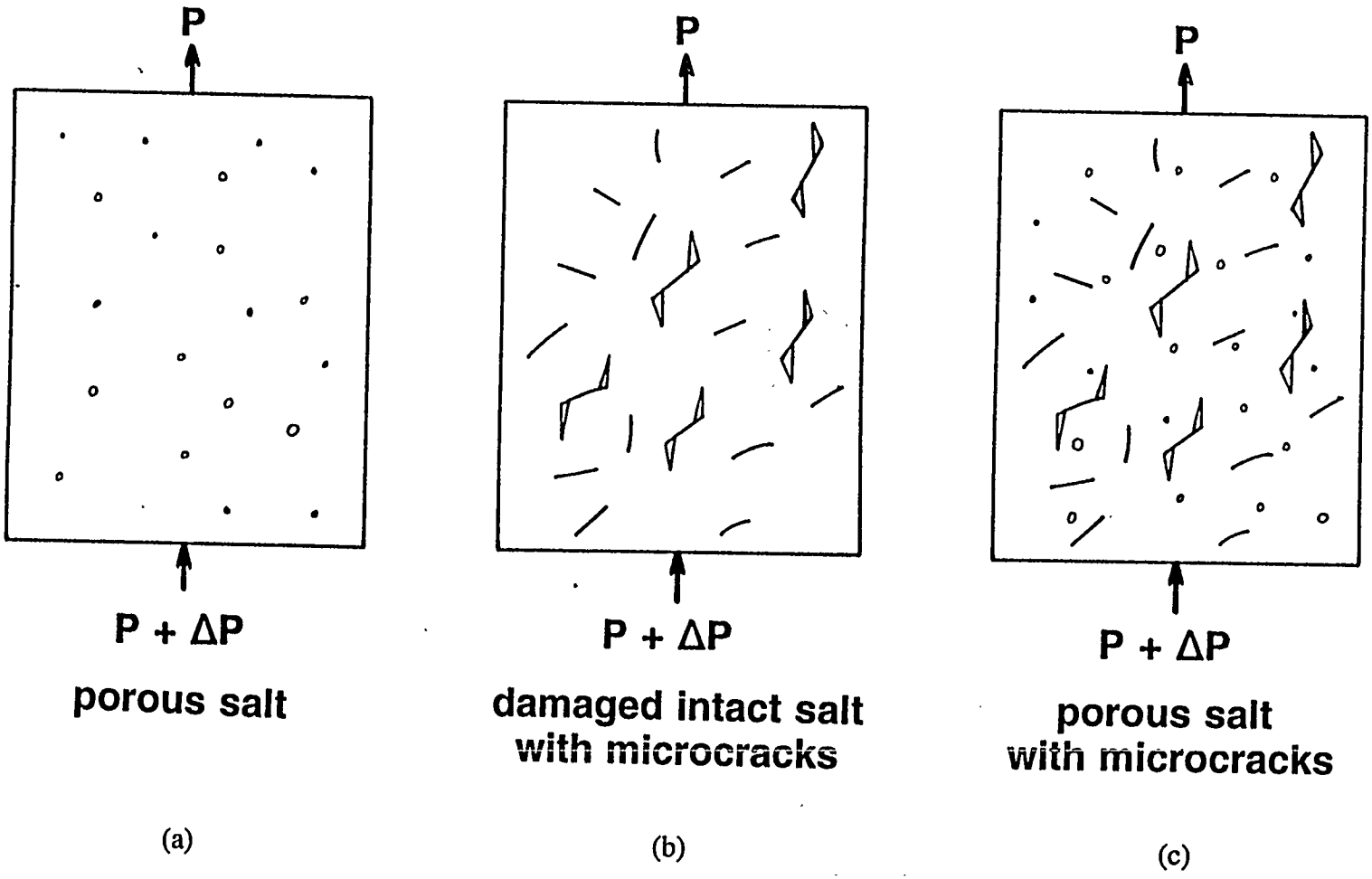

Figure 2. Schematics of rock salt materials whose permeabilities are modeled to establish relationships between permeability and damage: (a) porous salt, (b) damaged intact salt, and (c) porous salt with microcracks.

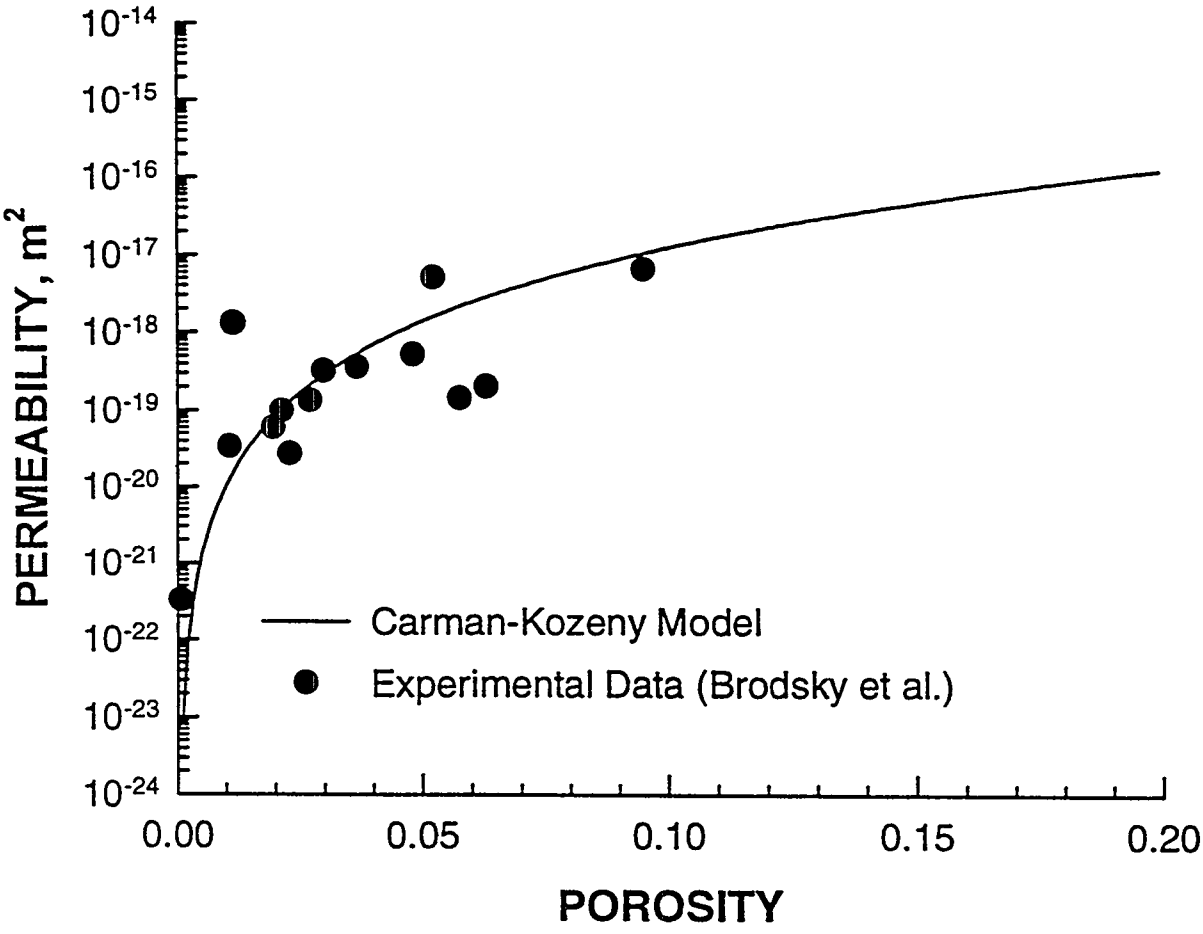

Figure 3. The Carman-Kozeny model fitted to the experimental data of compacted crushed salt from Brodsky et al. [22].

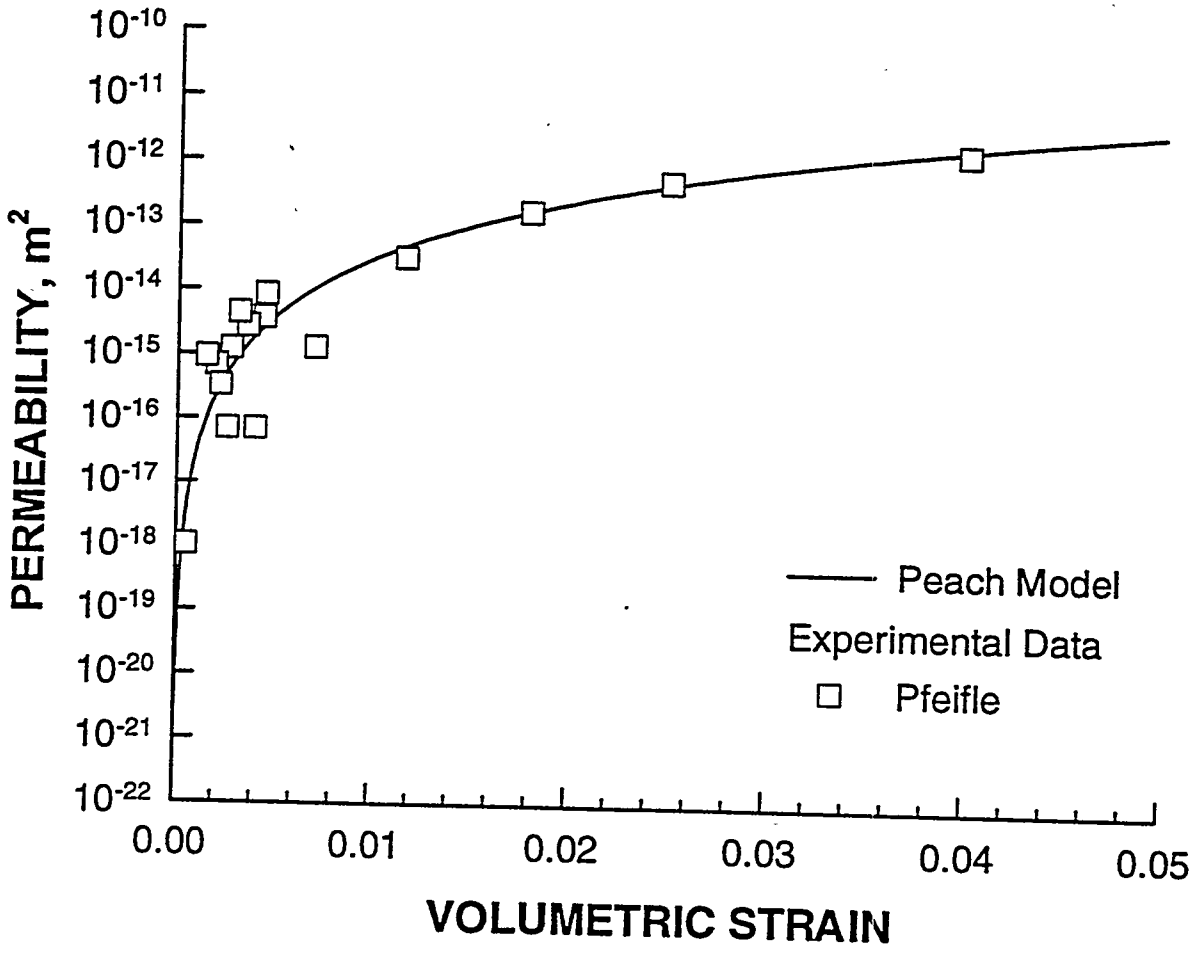

Figure 4. The Peach model [19] fitted to the experimental data of damaged intact salt from Pfeifle [23].

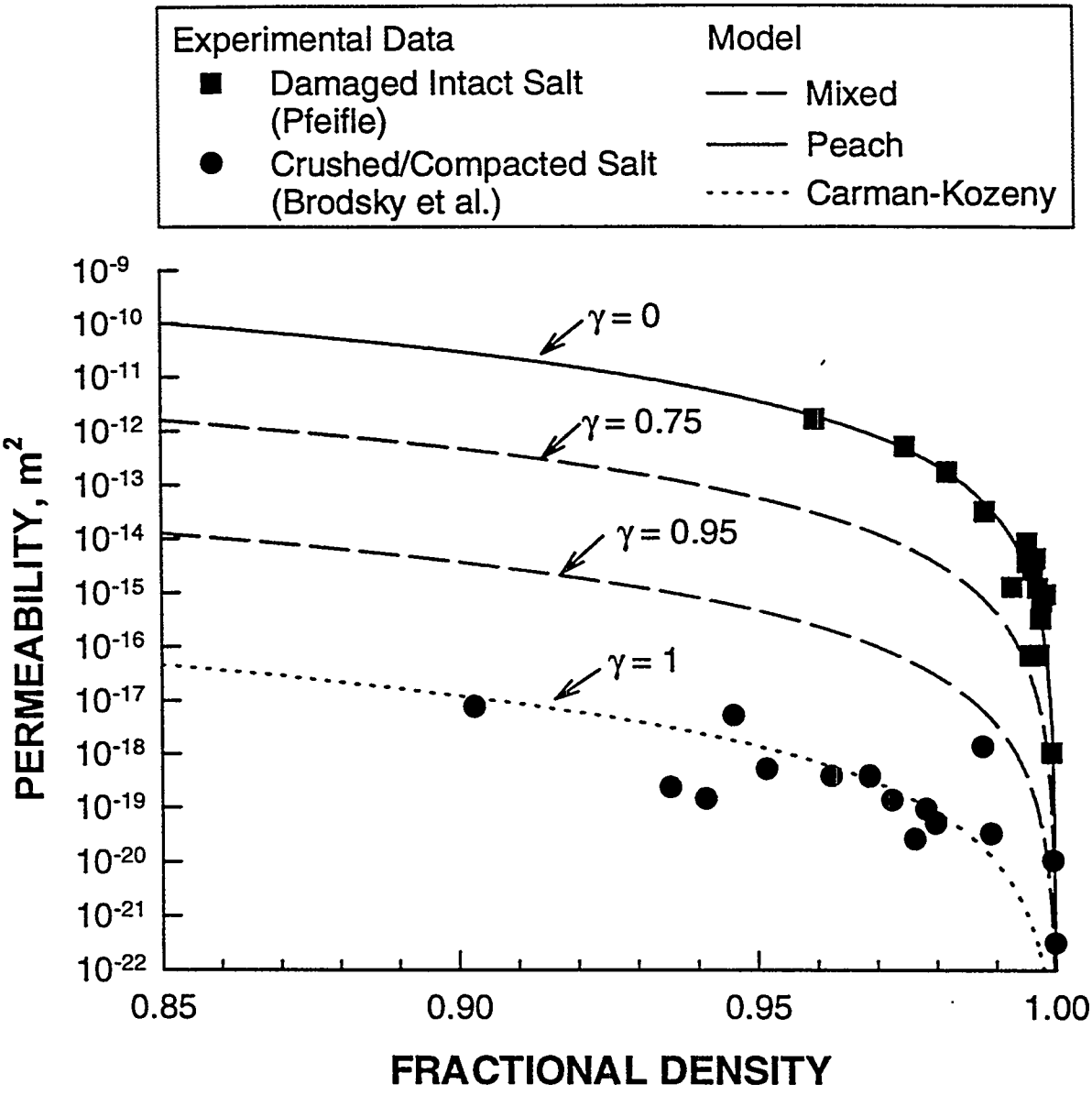

Figure 5. Calculations based on the proposed model for damaged porous materials show different dependence of permeability on porosity and volumetric strain, resulting in a dependence of permeability on the γ parameter. Experimental data are from Brodsky et al. [22] and Pfeifle [23].

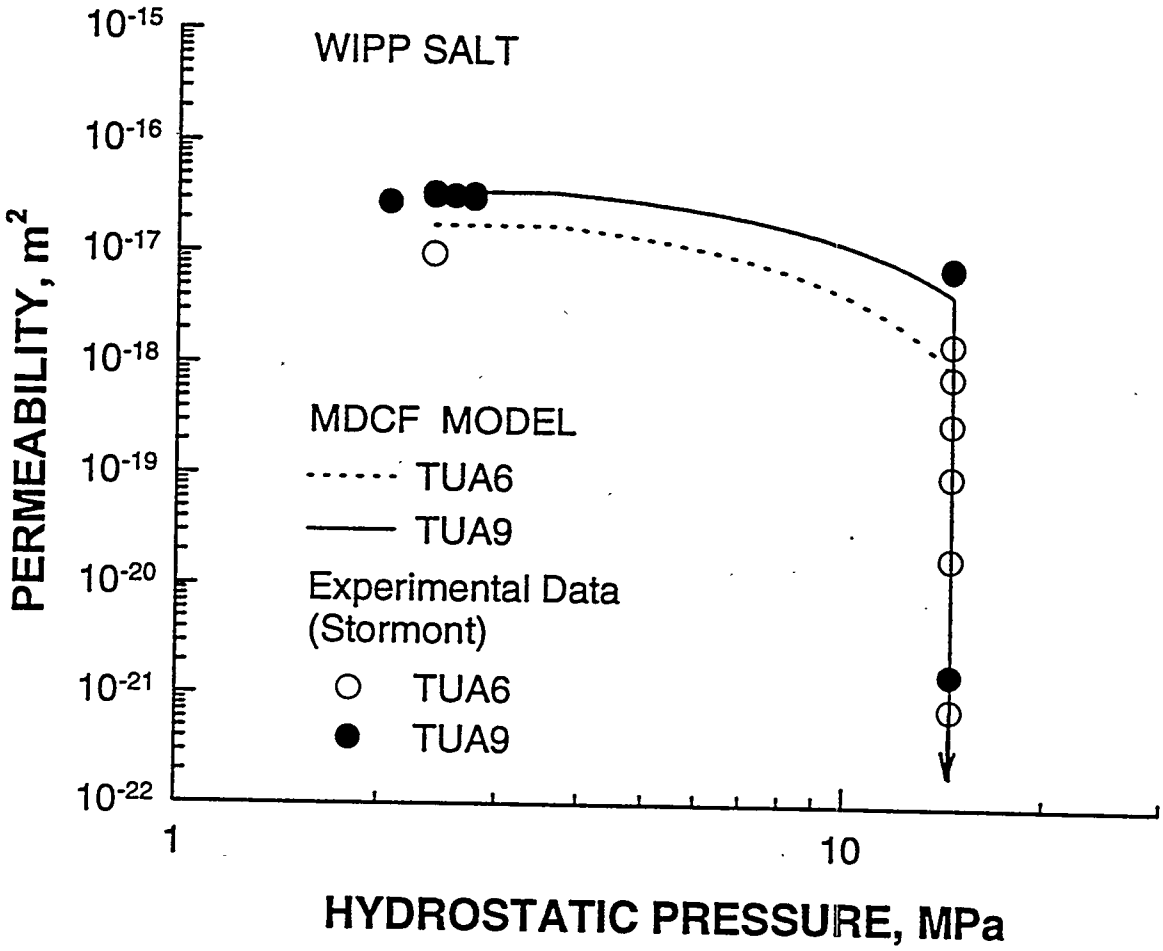

Figure 6. Comparison of calculated and measured values of permeability of WIPP salt as a function of hydrostatic pressures. The experimental data are from Stormont [20].

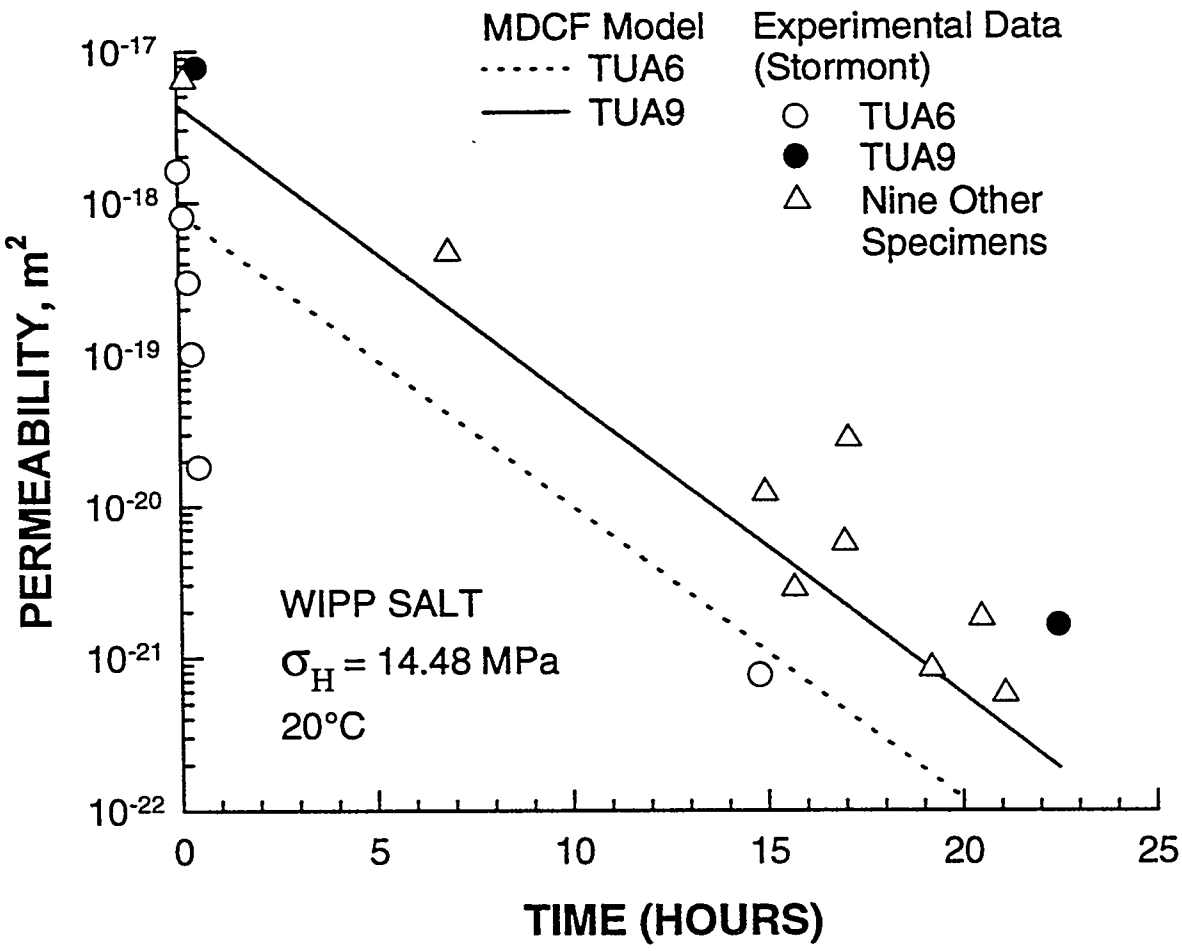

Figure 7. Comparison of calculated and measured values of permeability of WIPP salt as a function of time for healing under a hydrostatic stress, σ_H, of 14.48 MPa. The experimental data are from Stormont [20].

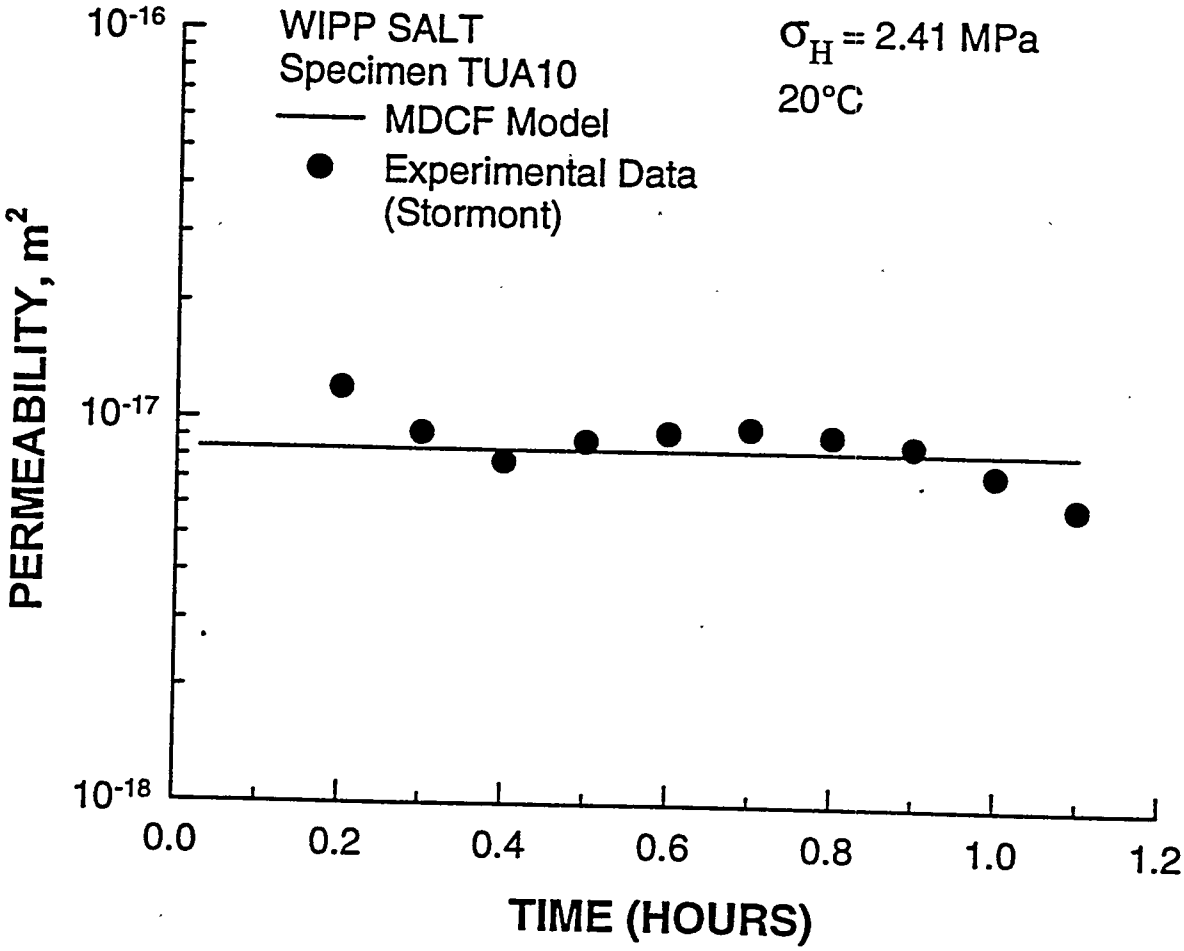

Figure 8. Comparison of calculated and measured values of permeability of WIPP salt as a function of time for healing under a hydrostatic stress, σ_H, of 2.41 MPa. The experimental data are from Stormont [20].

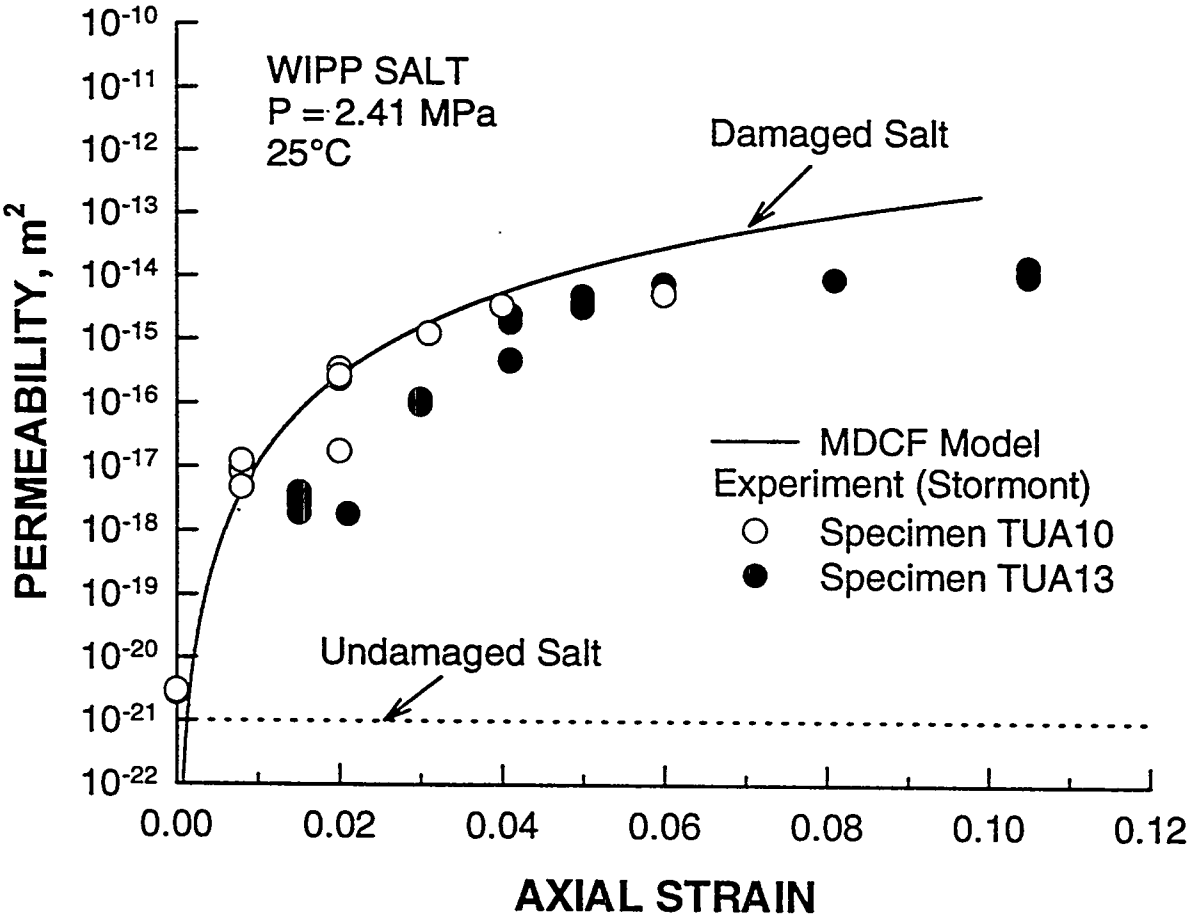

Figure 9. Calculated and measured values of permeability of WIPP salt subjected to triaxial compression under a confining pressure of 2.41 MPa. The experimental data are from Stormont [20].

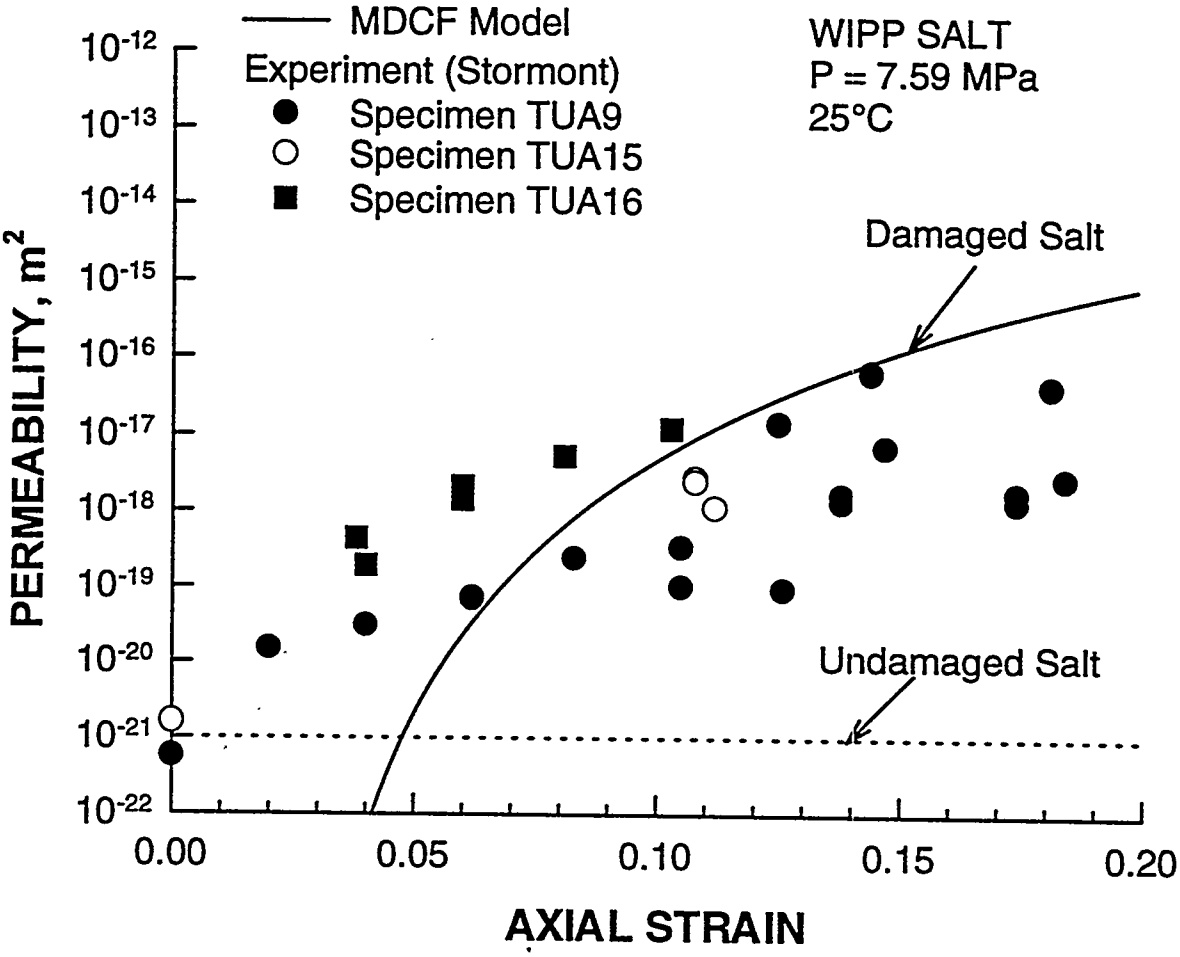

Figure 10. Calculated and measured values of permeability of WIPP salt subjected to triaxial compression under a confining pressures of 7.59 MPa. The experimental data are from Stormont [20].

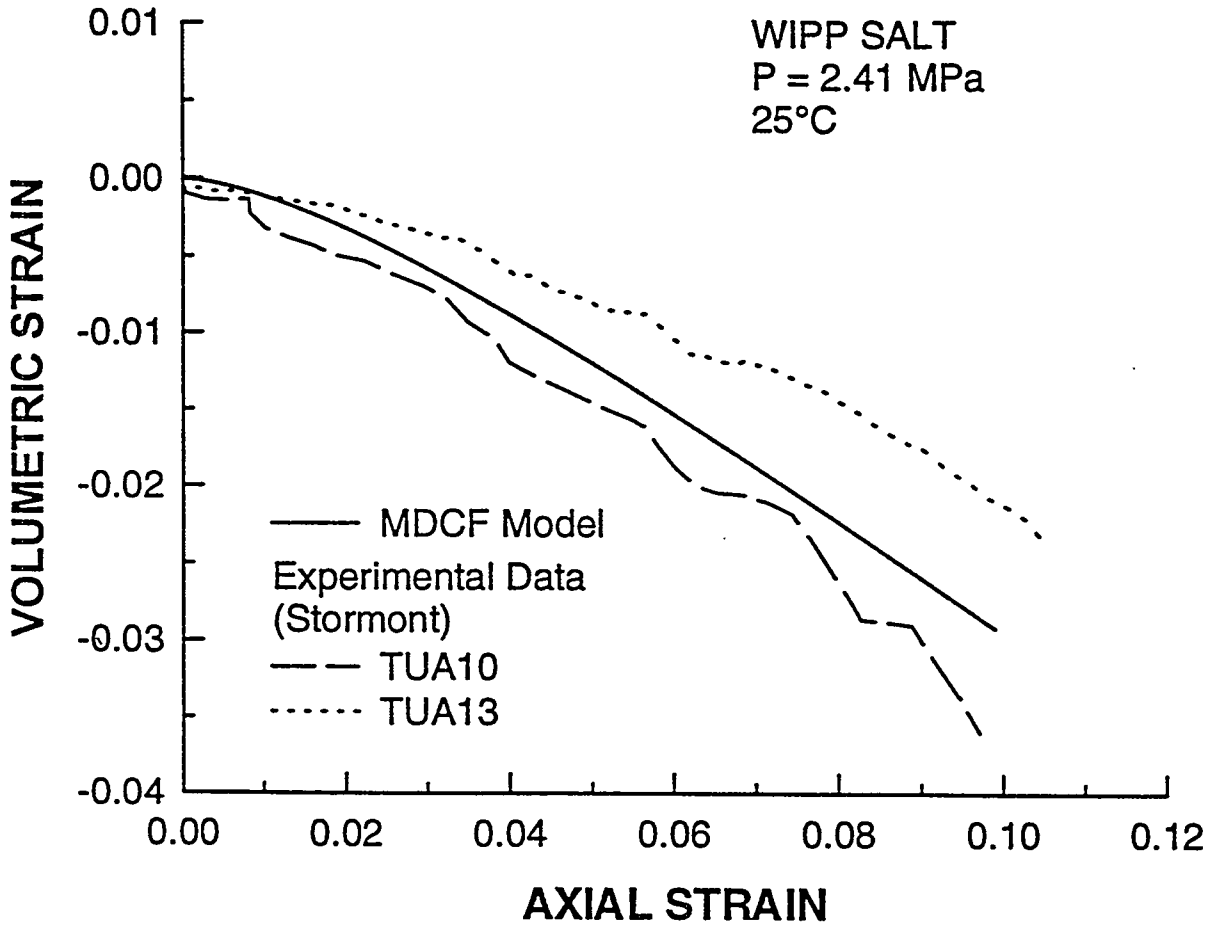

Figure 11. Comparison of calculated and measured inelastic volume strains during triaxial compression of WIPP under a confining pressures of 2.41 MPa. Experimental data are from Stormont [20].

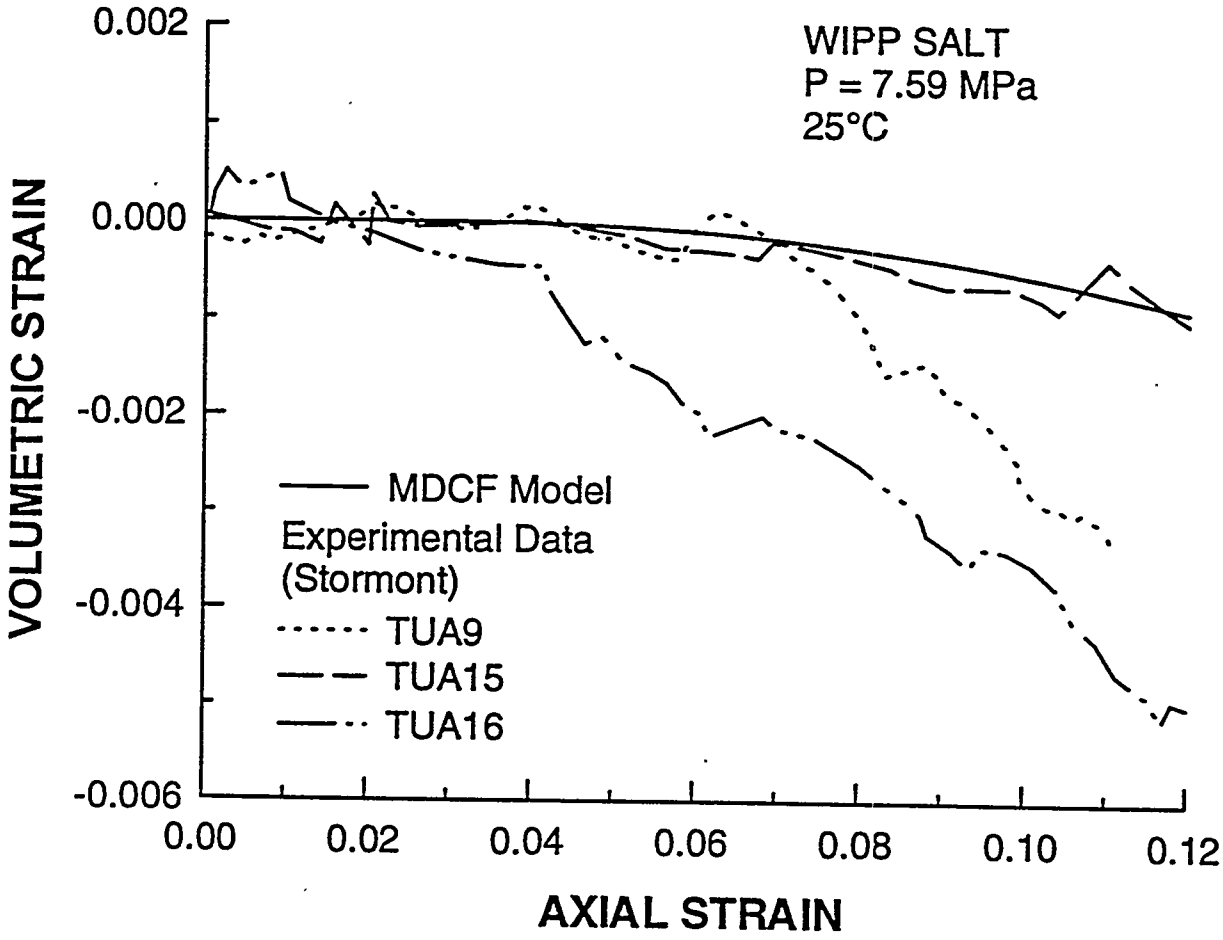

Figure 12. Comparison of calculated and measured inelastic volume strains during triaxial compression of WIPP under confining pressures of 7.59 MPa. Experimental data are from Stormont [20].